This is the accepted manuscript of the article that appeared in final form in **Acta Biomaterialia** 67 : 21-31 (2018), which has been published in final form at https://doi.org/10.1016/j.actbio.2017.12.014.

Antioxidant Functionalized Polymer Capsules to Prevent Oxidative Stress

Aitor Larrañaga[a,b], *Isma Liza Mohd Isa*[a], *Vaibhav Patil*[a], *Sagana Thamboo*[c], *Mihai* Lomora[a], *Marc A. Fernández-Yague*[a], *Jose-Ramon Sarasua*[b], *Cornelia G. Palivan*[c], *Abhay Pandit*[a,]*

[a] Centre for Research in Medical Devices (CÚRAM), National University of Ireland, Galway, Ireland

[b] Department of Mining-Metallurgy Engineering and Materials Science & POLYMAT, University of the Basque Country, Bilbao, Spain

[c] Chemistry Department, University of Basel, Basel, Switzerland

* Corresponding author: abhay.pandit@nuigalway.ie

Abstract:

Polymeric capsules exhibit significant potential for therapeutic applications as microreactors, where the bio-chemical reactions of interest are efficiently performed in a spatial and time defined manner due to the encapsulation of an active biomolecule (e.g., enzyme) and control over the transfer of reagents and products through the capsular membrane. In this work, catalase loaded polymer capsules functionalized with an external layer of tannic acid (TA) are fabricated via a layer-by-layer approach using calcium carbonate as a sacrificial template. The capsules functionalised with TA exhibit a higher scavenging capacity for hydrogen peroxide and hydroxyl radicals, suggesting that the external layer of TA shows intrinsic antioxidant properties, and represents a valid strategy to increase the overall antioxidant potential of the developed capsules. Additionally, the hydrogen peroxide scavenging capacity of the capsules is enhanced in the presence of the encapsulated catalase. The capsules prevent oxidative stress in an *in vitro* inflammation model of degenerative disc disease. Moreover, the expression of matrix metalloproteinase-3 (MMP-3), and disintegrin and metalloproteinase with thrombospondin motif-5 (ADAMTS-5), which represents the major proteolytic enzymes in intervertebral disc, are attenuated in the presence of the polymer capsules. This platform technology exhibits potential to reduce oxidative stress, a key modulator in the pathology of a broad range of inflammatory diseases.

Keywords: polymer capsules, layer-by-layer, enzyme encapsulation, oxidative stress, intervertebral disc

1. Introduction

Polymer capsules have traditionally been employed in the biomedical field as drug/gene/protein delivery vehicles.[1-3] Based on natural or synthetic polymers, these microstructures allow for the controlled spatiotemporal release of the encapsulated entities through polymeric systems that respond to single or multiple biologically relevant stimuli such as pH,[4] temperature[5] and cell biomarkers.[6] Apart from the aforementioned application, advances in biosciences and polymer synthesis have allowed the development of novel applications of polymer capsules in the biomedical field, including their use as microreactors, artificial organelles or cell mimics.[7-10]

As microreactors, polymer capsules accommodate active biomolecules (e.g., enzymes) inside their inner cavity that act *in situ* due to a continuous transfer of reagents and products through a shell/membrane with selective permeability.[11] Polymer vesicles (i.e., polymersomes), which are fabricated in the absence of a sacrificial template via self-assembly of amphiphilic block copolymers, have been widely employed as nanoreactors which facilitate single or cascade enzymatic reactions.[12-15] In these systems, the permeability of the membrane is finely tuned through the use of copolymers that self-assemble in compartments with a porous membrane,[16] the incorporation of biopores/protein channels in the membrane,[17-20] or the use of copolymers generating compartments whose membranes undergo conformational changes in response to specific stimuli.[21, 22]

Apart from polymersomes, controlled enzymatic reactions can also be performed within polymer capsules fabricated using a sacrificial template which act as a microreactor.[23-25] These polymer capsules are usually fabricated via a layer-by-layer (LbL) approach which involves the deposition of polymer layers through electrostatic, covalent or hydrogen bonding interactions on a sacrificial core template which is then removed.

Additionally, these systems can be further modified via the incorporation of nanoparticles or surface modification processes to yield polymer capsules with advanced functionalities.[26, 27] For the encapsulation of enzymes and the subsequent use as microreactors, calcium carbonate ($CaCO_3$) represents the most promising sacrificial template because of its inherent highly porous structure, ease of fabrication, high encapsulation efficiencies, which can be dissolved under mild conditions.[28] For this reason, several enzymatic reactions performed within polymer capsules, fabricated employing $CaCO_3$ as a sacrificial template, have been reported in the literature.[29-31] Despite the promising results observed in terms of encapsulation efficiencies, and enzyme activity, the translation to therapeutic applications has not yet been achieved and only a few studies have reported the use of these capsules in *in vitro* models.[32]

We developed polymer capsules that acted as antioxidant microreactors which scavenge reactive oxygen species (ROS). These systems were tested to prevent oxidative stress in an interleukin-1β (IL-1β) induced inflammation model of nucleus pulposus (NP). ROS such as hydrogen peroxide (H_2O_2), hydroxyl ($^{\cdot}OH$) and superoxide anion ($^{\cdot}O_2^-$) radicals are important signalling molecules that play a pivotal role in several cellular events (including gene expression, transcription factor activation, DNA damage, cellular proliferation and apoptosis).[33, 34] Under normal physiological conditions, the levels of ROS are efficiently regulated by several molecules and enzymes including glutathione, superoxide dismutase and catalase which exhibit antioxidant properties.[35] However, overproduction of ROS can overwhelm the antioxidant capacity of cells resulting in oxidative stress. The overproduction of ROS has been implicated in numerous disease pathologies (including cancer,[36, 37] neurodegeneration[38] and diabetes[39]). In degenerative disc disease, several *in vitro* and *in vivo* studies conducted on NP and annulus fibrosus (AF) cells have reported the activation of important signalling pathways including p38

mitogen-activated protein kinases (MAPK), extracellular signal-regulated kinases (ERKs), Jun amino-terminal kinases (JNKs), Akt, and nuclear factor-κB (NF-κB)[40] mediated by excessive ROS that induces senescence and apoptosis.[41] This promotes a catabolic and pro-inflammatory cell phenotype[42, 43] [as demonstrated by an up-regulated expression of proteolytic enzymes (matrix metalloproteinases (MMPs), and disintegrins and metalloproteinase with thrombospondin motifs (ADAMTSs)) and pro-inflammatory cytokines (IL-1β, interleukin-8 (IL-8), interleukin-6 (IL-6)]. This causes an imbalance in matrix homeostasis which results in degenerative disc disease which is one of the main causes of low back pain. Considering the socio-economic impact, 60-80% of the population of developed countries are affected by low back pain at some stage in their lives,[44, 45] the development of biomaterial-based systems to restore matrix homeostasis has gained significant interest in recent years.[46]

We hypothesize that polymer capsules with antioxidant properties will prevent oxidative stress and attenuate the expression of major proteolytic enzymes in an IL-1β induced inflammation model of NP. We fabricated polymer capsules loaded with catalase and functionalized with an external layer of TA via a LbL approach using $CaCO_3$ as a sacrificial template. Following comprehensive physico-chemical and functional characterization of the polymer capsules, their therapeutic efficacy was assessed on NP cells stimulated with IL-1β by analysing intracellular oxidative stress and the expression of matrix metalloproteinase-3 (MMP-3) and disintegrins and metalloproteinase with thrombospondin motif -5 (ADAMTS-5) (Figure 1).

2. Materials and Methods

2.1. Materials

$CaCl_2$, Na_2CO_3, NaCl, ethylenediaminetetraacetic acid (EDTA), poly(allylamine hydrochloride) (PAH) (M_w~58000 Da), dextran sulphate (DEX) from *Leconostoc* spp.

(DEX) (M_w>500000 Da), fluorescein 5(6)-isothiocyanate (FITC), FITC-dextran sulphate sodium salt (M_w~500000 Da), tannic acid (TA), bovine serum albumin (BSA), 50 wt.% hydrogen peroxide solution, $FeSO_4 \cdot 7H_2O$, 5,5-dimethyl-1-pyrroline *N*-oxide (DMPO), TRI Reagent®, Hank´s Balanced Salt Solution (HBSS), high glucose Dulbecco´s modified Eagle´s medium (HGDMEM), penicillin-streptomycin solution (P/S), foetal bovine serum (FBS), protease from *Streptomyces griseus*, collagenase from *Clostridium histolyticum*, fluorimetric hydrogen peroxide assay kit, Bradford reagent and protease inhibitor cocktail were purchased from Sigma-Aldrich (Ireland). AlamarBlue® cell viability reagent, live/dead® viability kit, rhodamine phalloidin, Hoechst staining solution, CellROX® green reagent, propidium iodide, BCA protein assay kit and SuperSignal West Pico Chemiluminescent substrate were purchased from ThermoFisher Scientific (Ireland). Human recombinant interleukin-1β cytokine was purchased from PeproTech (USA) whereas phosphatase inhibitor (PhosSTOP) was purchased from Roche (USA).

2.2. Fabrication and Characterization of Polymer Capsules

***Fabrication of Polymer Capsules*:**

Polymer capsules were fabricated via the LbL approach using $CaCO_3$ microparticles as a sacrificial template and PAH, DEX and TA as polyelectrolytes. For the fabrication of the sacrificial template, 0.66 mL of a 1 M Na_2CO_3 solution and 0.66 mL of a 2 mg/mL catalase solution were poured into an equal volume of 1 M $CaCl_2$ solution. In a particular case, FITC-labelled catalase was employed to demonstrate the successful encapsulation of the enzyme in the final polymer capsules. After vigorous stirring of these solutions for 30 seconds, the obtained dispersion was centrifuged and the particles were washed several times with a 0.005 M NaCl solution. Then, the particles were

suspended in a 2 mg/mL PAH solution of pH 6.5. After fifteen minutes of incubation, the particles were centrifuged and washed several times with a 0.005 M NaCl solution. Then, particles were suspended in a 2 mg/mL DEX solution at pH 6.5. This process was repeated until three layers of PAH and two layers of DEX were alternatively deposited. Finally, the particles were suspended in a 3 mg/mL TA solution at pH 6.5 and incubated for fifteen minutes. After the corresponding washing steps, the particles were submerged in a 0.1 M EDTA solution. After incubating for five minutes, the particles were recovered by centrifugation. This process was repeated four times to guarantee the complete removal of the sacrificial template. The resulting polymer capsules were washed several times with PBS prior to conducting physico-chemical and morphological characterization.

Physico-chemical and Morphological Characterization:

The amount of catalase loaded in the $CaCO_3$ template was determined via the Bradford method using BSA for the calibration curve.[47] The supernatant after the precipitation reaction between Na_2CO_3 and $CaCl_2$, as well as the supernatant from all the washing steps was collected and the amount of the enzyme was determined.

The ζ-potential of the particles after each polyelectrolyte deposition was collected from a minimum of ten runs, using a Malvern Instruments Zetasizer NanoZS90. Infrared spectra of the polyelectrolytes and capsules before and after the removal of the sacrificial template were collected on a Varian 660-IR spectrometer operating in the Attenuated Total Reflectance (ATR-FTIR) mode from Agilent Technology. The morphology of the sacrificial template and the polymer capsules was characterized by means of X-ray spectroscopy coupled scanning electron microscopy (EDX-SEM: Hitachi S-4700) and transmission electron microscopy (TEM) (Hitachi H-7500). In the

particular case of polymer capsules fabricated with FITC-labelled catalase, the presence of the enzyme within the capsules was confirmed by means of a laser confocal microscope (Olympus Fluoview 1000).

Stopped-flow experiments were performed using a single mixing stopped-flow apparatus (BioLogic SAS). A volume of 100 µL of a 10 mg/mL polymer capsules solution was automatically injected in a 1.5 mm light path FC-15 observation cuvette. Simultaneously, the same volume of a 20 mM H_2O_2 solution was injected and the absorbance at 240 nm was measured over a period of 200 seconds, using a sampling period of 10 milliseconds and a total flow rate of 4.5 mL/second. In this experiment, catalase in solution was used as a positive control at a concentration of 0.25 mg/mL. Before each injection, a visual inspection and manual agitation of the syringes containing the samples was carried out to avoid sedimentation of the polymer capsules. Stopped-flow data was acquired and presented as an average of at least five injections for each sample.

A fluorimetric hydrogen peroxide assay kit was employed to determine the H_2O_2 scavenging capacity of the capsules. Five or twenty µL of polymer capsule dispersion was added to 1 mL of a 10 µM or 50 µM H_2O_2 solution (final concentration of capsules in the reaction volume was 100 or 400 µg/mL). After ten minutes of reaction, 50 µL of each sample was added to a well in a 96-well plate together with another 50 µL of master mix containing horseradish peroxidase and red peroxidase substrate. After incubating for 20 minutes sheltered from light, the fluorescence intensity was measured (λ_{ex} 540 nm/λ_{em} 590 nm) to determine the H_2O_2 concentration in the solution.

Electron paramagnetic resonance (EPR) measurements were carried out in a Bruker CW EPR Elexsys-500 spectrometer to determine the hydroxyl radical (˙OH) scavenging capacity of the developed polymer capsules. All EPR spectra were recorded at 298 K

employing the following acquisition parameters: microwave power 2 mW, modulation frequency 100 kHz, modulation amplitude 1 G, receiver gain 60 dB. DMPO served as a spin trap and the Fenton reaction was utilized to generate $^{\cdot}OH$ radicals.[16] Briefly, 70 µL of PBS was mixed with 10 µL of 1 mM $FeSO_4$, 10 µL of 10 mM or 1 mM H_2O_2 and the produced free radicals were trapped by the addition of 10 µL of a 1 M solution of DMPO. The same reaction was performed in the presence of polymer capsules (final concentration of capsules in the reaction 10 mg/mL, 4 mg/mL, 2 mg/mL or 1 mg/mL), catalase (final concentration of catalase 50 µg/mL, 25 µg/mL, 10 µg/mL or 5 µg/mL) or tannic acid (final concentration of tannic acid 450 µg/mL, 225 µg/mL, 90 µg/mL or 45 µg/mL). The EPR spectra were collected 10 minutes after mixing all the reagents. The double integral of the EPR spectrum was used to calculate the relative concentration of the OH radical.

2.3. *In Vitro* Studies

***NP Cell Isolation and Culture*:**

NP cells were isolated following the protocol described previously.[46] Discs from five-month-old bovine tails were collected immediately after sacrifice. After dissecting the surrounding soft tissue, the discs were cut into four sagittal sections. The NP tissues were then harvested from each section and washed twice using Hank's buffered salt solution (HBSS) and once with blank high-glucose DMEM (HGDMEM). NP tissues were subsequently digested with a 0.19% Pronase solution in HGDMEM for one hour at 37 ºC in a humidified atmosphere of 5% CO_2 under mild shaking. Afterwards, the tissues were washed three times with complete (10% FBS+1% P/S) HGDMEM to inhibit the activity of Pronase and then suspended in 0.025% collagenase type IV solution in complete HGDMEM. The mixture was incubated overnight at 37 ºC in a

humidified atmosphere of 5% CO_2 under mild shaking. The suspensions were filtered through a 70 µm cell strainer and a pellet of NP cells was obtained by centrifugation at 1,200 rpm for eight minutes. The pellets were finally washed once with complete HGDMEM. Cells were transferred to tissue culture flasks and the media was changed every three days until confluence. All the experiments were carried out after passaging the cells once (all experiments were performed at passage one) and three biological (different tails) and technical replicates were employed for statistical purposes.

Seeding of NP Cells:

NP cells were seeded at a density of 150,000 cells/cm^2 in complete HGDMEM for 24 hours. After this time, the media was replaced by fresh complete HGDMEM or fresh complete HGDMEM containing 10 ng/mL of IL-1β to create an inflammatory milieu that mimics the disease environment of the IVD.[46, 48] Polymer capsules were added after 90 minutes at a final concentration of 100 µg/mL or 400 µg/mL.

***Metabolic Activity and Viability of NP Cells*:**

The metabolic activity and viability of NP cells in the presence of polymer capsules were evaluated using the alamarBlue® assay and Live/Dead® staining kit, respectively. For the metabolic activity, at the selected time points (12 hours or 72 hours), media was removed and cells were washed with HBSS and subsequently incubated for six hours at 37 ºC in fresh complete media with alamarBlue® (10% v/v). Finally, 100 µL of the assay media was transferred to a 96-well plate, the absorbance was read at 550 and 595 nm on a microplate reader (VarioskanFlash) and the percentage reduction of the dye was calculated. For viability studies, after 72 hours, media was aspirated and cells were washed twice with HBSS. Then, cells were incubated with HBSS containing 4 µM of

ethidium homodimer-1 and 1 μM of calcein for 30 minutes at room temperature. Finally, cells were washed twice in HBSS and observed under a laser confocal microscope (Olympus Fluoview 1000).

***Internalization of Polymer Capsules*:**

In this experiment, polymer capsules fabricated with FITC-dextran were employed. At the selected time point (24 hours), media was removed and the cells were fixed with 4 % paraformaldehyde. After permeabilization of the membrane with 0.5% Triton X-100 in PBS, actin filaments and the nuclei of cells were stained with Rhodamine Phalloidin (0.066 μM) and Hoechst (2 μM) staining solutions, respectively. Samples were observed with a laser confocal microscope (Olympus Fluoview 1000).

Internalization of FITC-dextran capsules was also analysed by flow cytometry. At the selected time point (24 hours), NP cells were detached with 0.25 % trypsin/ 0.02 % EDTA and suspended in FACS buffer at a cell density of 10^6 cells/mL. Cells were stained with propidium iodide (PI) (0.1μg/mL) prior to analysis. Flow cytometry analysis was done using an Accuri C6 sampler flow cytometer (Becton Dickinson Bioscience). Posterior data analysis was performed using FlowJo software (TreeStar Inc.). Typical gating strategies were done by means of gating size (Forward Scatter_FSC) versus granularity (Side Scatter_SSC), doublet exclusion based on FSC-H versus FSC-A, and dead cell exclusion by gating on negative PI fluorescence population.

***Oxidative Stress Measurements*:**

To measure the presence of ROS in NP cells, CellROX® Green reagent was employed. After an incubation period of 72 hours with the polymer capsules, the media was

replaced by HBSS containing 5 µM of CellROX® Green reagent and incubated for 30 minutes at 37 ºC. The reagent was then aspirated and the cells were washed three times with HBSS. Finally, cells underwent a fixing and staining (Rhodamine Phalloidin for actin filaments and Hoechst staining solution for nuclei) process as described above prior to analysis via laser confocal microscopy (Olympus Fluoview 1000). Observation of CellROX® green reagent was performed at λ_{ex}=485 nm/λ_{em}=520 nm and an exposure time of 250 ms; observation of nuclei was performed at λ_{ex}=352 nm/λ_{em}=461 nm and an exposure time of 150 ms; observation of actin filaments was performed at λ_{ex}=540 nm/λ_{em}=565 nm and an exposure time of 250 ms. For quantification purposes, a single z slice of confocal images was obtained from five microscopic views of each three technical replicates and the images were analysed by Image J software version 1.48 (NIH, Bethesda, MD, USA). The CellROX® positively stained cells were quantified and expressed as a percentage of the total cells

mRNA Expression of MMP-3 and ADAMTS-5:

After an incubation period of 72 hours with the polymer capsules, total RNA was extracted using TRI Reagent® and miRNeasy mini kit (Qiagen) following the manufacture´s protocol. Total RNA (100 ng/µL) was reverse transcribed using random primer (Promega) and reverse transcriptase (Promega) in a 20 µL reaction mixture using PTC DNA Engine System (PTC-200, Peltier Thermal Cycler, MJ Research Inc.). The cDNA products were amplified using SYBR green (Qiagen) PCR Master Mix (Promega) and the corresponding pair of primers (Eurofins) (Table S1). Reactions were conducted using StepOnePlus Real-Time PCR System (Applied Biosystems) and the results analysed using $2^{-\Delta\Delta Ct}$ method and presented as fold change (with respect to NP cells in fresh complete HGDMEM without IL-1β) normalized to 18S.

IL-6 Secretion:

After an incubation period of 12 hours or 72 hours with polymer capsules, the media was collected and the level of IL-6 was checked by the DuoSet ELISA kit (R&D Systems) following the protocol recommended in the kit.

Western Blotting:

After an incubation period of 15 minutes or 90 minutes with polymer capsules, cells were lysed in a Radioimmunoprecipitation assay (RIPA) buffer (50 mM Tris–HCl, pH 8.0, 150 mM NaCl, 0.02% sodium azide, 0.1% sodium dodecyl sulphate (SDS), 1% Nonidet P-40, 0.5% sodium deoxycholate) with protease inhibitor cocktail (1:100), phenylmethylsulfonylfluoride (1:50) and phosphatase inhibitor (1:10). Protein concentration in cell lysates was determined using a BCA protein assay kit. An equal amount of protein from each sample was separated by 10% SDS polyacrylamide gel electrophoresis and transferred to a polyvinylidene difluoride (PVDF) membrane. The membrane was blocked with either 5% milk or 5% BSA depending upon the suitability of primary antibodies to avoid non-specific binding of antibodies. Blots were probed overnight at 4°C with 1:2,000 rabbit anti-P-NF-κB p65 (Ser536) (93H1) (Cell signalling, 3033s), mouse anti-NF-κB p65 (F-6) (Santacruz biotech, sc-8008) and 1:15,000 anti-β-actin (Sigma, A5441). Next, horseradish peroxidase-conjugated secondary goat anti-rabbit or goat anti-mouse antibodies (prepared in 5% milk or 5% BSA at 1:10,000) were applied followed by enhanced chemiluminescence detection.

2.4. Statistical Analysis

All quantitative data related to the fabrication and characterization of polymer capsules are presented as the mean ± standard deviation (SD). For *in vitro* studies three biological and technical replicates were employed and the results are presented as the mean ± standard error. The statistical difference between groups was tested by *t*-test and one-way analysis of variance (ANOVA) at a confidence level of 95% ($p < 0.05$).

3. Results and Discussion

3.1. Fabrication of Catalase-Loaded and Tannic Acid-Functionalized Polymer Capsules

For the fabrication of polymer capsules, the $CaCO_3$ sacrificial template was first synthesized by colloidal crystallization from a supersaturated solution.[49] This process resulted in the formation of catalase-loaded $CaCO_3$ spherical microparticles with a diameter size of 2-3 µm (Figure 2a and 2b). Catalase was loaded into the $CaCO_3$ template via a co-precipitation approach that has been reported to result in a five-fold higher encapsulation efficiency compared to physical adsorption methods.[50] The encapsulation efficiency of catalase in the $CaCO_3$ template was 97.8%, as determined by the Bradford assay (Figure S1). Considering that protein loss during EDTA treatment is inversely proportional to the size of the encapsulated entity and the number of polymer layers,[51] the amount of catalase (M_{CAT} 250 kDa) in the final polymer capsules is sufficient to effectively scavenge H_2O_2. The template initially showed a negative surface charge at pH 6.5 due to the presence of catalase that has an isoelectric point (pI) of 5.4. Accordingly, for the LbL approach, the template was first incubated with PAH and the surface charge shifted from the initial value of -6.5±2.5 mV to 4.7±1.2 mV (Figure 2e). Thereafter, the particles were alternatively incubated in DEX and PAH

solutions and the surface charge changed from negative to positive as expected. After the deposition of five layers (PAH-DEX-PAH-DEX-PAH), particles were functionalized with TA which, apart from the electrostatic interaction with PAH, forms hydrogen bonds through the formation of hydrogen-centred complexes with the primary amines of PAH.[52] Finally, the particles were immersed in a 0.1 M EDTA solution to remove the $CaCO_3$. As observed by SEM and TEM, polymer capsules retained their spherical shape and were hollow after treatment with EDTA due to their slightly collapsed appearance (Figure 2c and 2d). To confirm the complete removal of $CaCO_3$ from the polymer capsules, FTIR (Figure 2f) and EDX (Figure S2) spectra were acquired. The $CaCO_3$ FTIR spectrum was characterized by the presence of two main bands centred at 1384 cm^{-1} and 870 cm^{-1} that correspond respectively to asymmetric ν_3 and asymmetric ν_4 vibrations of CO_3. Before the treatment with EDTA, these two bands were still present in the spectrum together with bands at 1492 cm^{-1} and 1591 cm^{-1} and bands in the 1000 cm^{-1}-1300 cm^{-1} range associated with the bending vibration of primary amines from PAH and the vibrations of C-O, C-C bonds and S=O asymmetrical vibration from DEX respectively. However, after treatment with EDTA, the bands at 1384 cm^{-1} and 870 cm^{-1} associated with the $CaCO_3$ sacrificial template were not observed in the FTIR spectrum and only those bands at 1492 cm^{-1} and 1591 cm^{-1} and in the 1000 cm^{-1}-1300 cm^{-1} range corresponding to PAH and DEX respectively were detected.

In the EDX spectra, no signal associated with Ca was observed after the EDTA treatment, confirming the complete removal of the sacrificial template (Figure S2). To confirm the presence of catalase in the polymer capsules, FITC-labelled catalase was utilised in the fabrication process. As observed in fluorescent micrographs (Figure 2g and Figure 2 h), catalase was present within the polymer capsules at the end of the

fabrication process. Moreover, after incubating the samples for three days in PBS at 37 ºC, no significant decrease in the fluorescence intensity was observed, highlighting the stability of the polymer capsules under physiological conditions and the lack of permeability of their membrane towards encapsulated FITC-catalase (Figure S3).

3.2. H_2O_2 and $^{\cdot}OH$ Scavenging Capacity of Polymer Capsules

To demonstrate the H_2O_2 scavenging ability of the developed capsules, firstly stopped-flow measurements were conducted using a 10 mM H_2O_2 concentration. In this experiment, the absorbance of the solution at 240 nm, which is proportional to the H_2O_2 concentration, was continuously monitored over a period of 200 seconds. Free catalase (catalase in solution) was employed as a positive control. As observed in Figure 3a, the concentration of H_2O_2 rapidly decreased in the presence of 0.25 mg/mL free catalase due to the well-known H_2O_2 scavenging capacity of this enzyme.[53] Empty capsules (polymer capsules without catalase and not functionalized with TA) acted as negative controls. In this case, the concentration of H_2O_2 was maintained in the presence of 5 mg/mL of empty capsules, indicating that the polyelectrolytes employed for their fabrication did not have any capacity to scavenge H_2O_2 from the solution *per se*. In contrast, the concentration of H_2O_2 in the presence of capsules loaded with catalase (CAT) and further functionalized with TA (TA+CAT) decreased in a time dependent manner (Figure 3a). As expected, H_2O_2 degradation by catalase-loaded capsules occurred more slowly than in the case of free enzyme. It has to be considered that the multilayer polymeric shell acts as a barrier between the substrate and the enzyme, and so the substrate has to cross the polymeric shell following a Fickian diffusion mechanism.[54, 55] Those capsules loaded with catalase and functionalized with TA (TA+CAT) showed a slightly higher scavenging capacity than the capsules that were

not functionalized with TA (CAT), suggesting that TA may additionally scavenge H_2O_2 and contribute to the overall H_2O_2 scavenging capacity of these capsules.

To analyse the H_2O_2 scavenging capacity of the developed systems in biologically relevant H_2O_2 concentrations,[56] a fluorimetric hydrogen peroxide assay kit was used. In this experiment, polymer capsules with a concentration of 100 µg/mL or 400 µg/mL and a H_2O_2 concentration of 10 µM or 50 µM were used (Figure 3b and Figure S4). The concentration of H_2O_2 was maintained in the presence of empty capsules, confirming that these capsules did not possess the capacity to scavenge H_2O_2 *per se*. However, the concentration of H_2O_2 significantly decreased in the presence of 400 µg/mL tannic acid-functionalized capsules (TA), capsules loaded with catalase (CAT) and capsules loaded with catalase and further functionalized with TA (TA+CAT). Here the concentration of H_2O_2 dropped from 10±0.2 µM to 4.9±0.1, 2.4±0.1and 2.7±0.5 µM respectively in the presence of TA, CAT and TA+CAT capsules.

Similarly, at the highest H_2O_2 concentration, the H_2O_2 concentration dropped from 50±1.3 µM to 41.7±0.7, 25.9±0.2 and 17.6±0.4 µM respectively in the presence of TA, CAT and TA+CAT capsules. From this experiment, it can be concluded that TA can scavenge H_2O_2 by itself, which has been previously reported in the literature.[57] Additionally, the H_2O_2 scavenging capacity of the capsules is enhanced in the presence of the encapsulated catalase. To further prove the stability of the encapsulated catalase, the capability of the capsules to scavenge H_2O_2 after being submerged in PBS at 37 ºC for one and three days was also assessed. As depicted in Figure S5, polymer capsules retain their initial activity (relative activity with respect to the activity of the capsules at day 0 > 95%) after being incubated for one day. However, the relative activity dropped to 68% ([H_2O_2] 10 µM) and 40% ([H_2O_2] 50 µM) when the capsules were incubated in PBS for three days.

The capacity of the developed capsules to scavenge ·OH, which represents an important oxidant species within the ROS family, was analysed by EPR employing a Fenton reaction ($Fe^{2+} + H_2O_2 \rightarrow Fe^{3+} + {}^{\cdot}OH + OH^-$) to generate ·OH. Considering the short half-life of ·OH in solution at room temperature (100 µs), DMPO was used as a spin trap to form a DMPO/·OH adduct with a half-life of around 15 minutes.[16, 58] The EPR spectrum of the DMPO/·OH adduct is characterized by four peaks with peak intensity ratios of 1:2:2:1 and hyperfine coupling constants a_N and a_H for ^{14}N and ^{1}H of 14.9 G. As a first approach, the Fenton reaction was performed with a final concentration of H_2O_2 of 1 mM in the presence of catalase or tannic acid in solution (Figure S6). Tannic acid showed a potent scavenging capacity towards hydroxyl radicals. In this sense, after the incorporation of 450 µg/mL (260 µM) of tannic acid, no signal was detected by EPR. Even the addition of 45 µg/mL (26 µM) of tannic acid resulted in a clear decrease in the double integral of the EPR spectrum, which is proportional to the OH radical concentration. In contrast, incorporation of catalase did not have any significant effect on the acquired spectra at the concentrations studied. Next, the Fenton reaction (final concentration of H_2O_2 of 1 mM) was performed in the presence of different concentrations of empty capsules, capsules functionalized with TA, capsules loaded with catalase (CAT) and capsules loaded with catalase and further functionalized with TA (TA+CAT) (Figure 3c). The EPR signal intensity remained constant in the presence of various concentrations of empty and CAT capsules (neither of which were functionalized with TA) and no significant change in the OH radical concentration was observed (Figure 3d). Conversely, the signal intensity decreased in a concentration-dependent manner in the presence of capsules functionalized with tannic acid (TA+CAT capsules). In this situation, the OH radical concentration decreased steadily up to a capsule concentration of 4 mg/mL. A trend similar to the one reported for the Fenton

reaction performed with a final H_2O_2 concentration of 1 mM was observed when the reaction was performed with a final H_2O_2 concentration of 100 µM (Figure S7 and Figure S8). Tannic acid is a natural polyphenol which has been shown to exhibit considerable capability to scavenge several free radicals and pro-oxidant molecules thanks to its redox properties, which allow it to act as a reducing agent, hydrogen donor and quencher of singlet oxygen.[59-62] Accordingly, and in view of the EPR results presented herein, functionalization of the polymer capsules with an external layer of tannic acid is a valid strategy to confer ·OH scavenging capabilities and to increase the overall antioxidant potential of the developed capsules.

3.3. Interaction of Polymer Capsules with NP Cells *In Vitro*

In the present work, we used primary NP cells isolated from bovine tails as a cell source. These chondrocyte-like cells are commonly embedded in a network of collagen fibrils (mainly collagen type II) together with a proteoglycan-rich gelatinous matrix which is surrounded by the AF.[63] This cell type was chosen to study the mechanisms associated with degenerative disc disease due to its importance in preserving the metabolic homeostasis of the disc by balancing the synthesis of extracellular matrix (ECM) components and the catabolic activity by degradative enzymes such as proteases.

NP cells were stimulated with 10 ng/mL of the pro-inflammatory cytokine IL-1β. Western blotting showed the activation of the noncanonical nuclear factor-κb (NF-κB) pathway by IL-1β in NP cells (Figure S9a and Figure S9b). Addition of polymer capsules did not significantly interfere with this mechanism at the selected time-points. The increased secretion of IL-6 in the supernatant corroborated with the stimulation of NP cells by IL-1β (Figure S9c). In this case, a slight but significant reduction in the

levels of IL-6 was observed in cells treated with polymer capsules. Overall, the results from western blot experiments, together with the secretion of IL-6, validates our inflammation model, irrespective of the presence of polymer capsules. In response to IL-1β, IκB kinase complex (IKK) is activated, leading to a phosphorylation-induced degradation of IκB. This enables the translocation of NF-κB into the nucleus and the subsequent activation of gene transcription (Figure S9d).[64, 65]

Stimulation with IL-1β has been reported to aggravate oxidative stress in cells from the intervertebral disc (IVD).[66] Additionally, IL-1β which is highly expressed in the degenerative disc is involved in multiple pathological processes including inflammation, matrix degradation, angiogenesis and innervation.[67] Therefore, stimulation with IL-1β represents a more clinically relevant stimulus to induce oxidative stress than the direct addition of hydrogen peroxide.[41]

3.3.1. Metabolic Activity and Viability of NP Cells

Figure 4a shows the metabolic activity of IL-1β-stimulated NP cells in the absence or presence of 400 μg/mL of catalase-loaded (CAT) or catalase-loaded and tannic acid-functionalized (TA+CAT) polymer capsules. The metabolic activity was normalized at each time-point with respect to the metabolic activity of NP cells seeded in the absence of polymer capsules and IL-1β. As observed in Figure 4, neither stimulation with IL-1β nor the addition of polymer capsules had a detrimental effect on the metabolic activity of NP cells. A metabolic activity greater than 85% was recorded for all conditions studied. NP cells also maintained their normal metabolic activity when they were seeded in the presence of different concentrations of polymer capsules and in the absence of IL-1β (Figure S10). These results were supported by viability experiments

(Figures 4b-e), where no marked decrease in the viability of NP cells was observed in the presence of either IL-1β or the polymer capsules.

3.3.2. Cell Uptake

To determine whether the developed capsules were uptaken by NP cells, polymer capsules were fabricated using FITC-labelled dextran instead of DEX. Accordingly, polymer capsule internalization could be qualitatively and quantitatively analysed via fluorescent microscopy and flow cytometry, respectively. As observed in the fluorescent micrographs (Figure 4f and Figure 4g), FITC-labelled polymer capsules are co-localized with actin filaments, suggesting that they are internalized by NP cells. These qualitative results were further confirmed by flow cytometry measurements. After the corresponding gating strategy to exclude dead cells, two cell populations were observed: cells with FITC-labelled polymer capsules and cells without FITC-labelled polymer capsules (Figure 4h). This analysis indicated that over 70% of NP cells had internalized FITC-labelled polymer capsules after 24 hours of incubation. It has been previously reported that several cell types (including macrophages, ovarian carcinoma 2008 and C13 cell lines, smooth muscle cells and neuroblastoma B50 cells) are able to internalize polymer capsules fabricated via the LbL approach using $CaCO_3$ sacrificial templates.[68-72]

3.3.3. Intracellular Oxidative Stress Attenuation in the Presence of Capsules

CellROX® Green reagent, which is a cell-permeable reagent that becomes fluorescent upon oxidation with ROS, was employed to determine intracellular oxidative stress in NP cells. As observed in Figure 5a and Figure 5b, stimulation of NP cells with 10 ng/mL of IL-1β resulted in a significant increase in the CellROX® positively stained

cells. In this sense, less than 10% of NP cells were positively stained with CellROX® under basal conditions, whereas 67% of NP cells were positively stained after stimulation with IL-1β. Following treatment with 400 µg/mL of catalase- loaded (CAT) capsules, the amount of positively stained NPs decreased to 46%. The treatment with 400 µg/mL of catalase-loaded and tannic acid-functionalized (TA+CAT) capsules further decreased this percentage to 3%.

Previous studies have reported that treatment with antioxidant compounds is an efficient strategy to prevent or reduce oxidative stress in H_2O_2-stimulated NP cells.[73, 74] As an illustration, NP cells isolated from rats were preincubated with 10 µM or 50 µM of pyrroloquinoline quinone and subsequently stimulated with 200 µM of H_2O_2.[73] It was observed that the increase in intracellular ROS due to H_2O_2 stimulation was partially inhibited by the treatment with pyrroloquinoline quinone. In another example, Cheng *et al.*[74] employed 500 µM ferulic acid to prevent oxidative stress in rabbit NP cells stimulated with 100 µM of H_2O_2.

Unlike the aforementioned studies, we employed IL-1β, which is highly expressed in the degenerative disc and thus represents a clinically more relevant stimulus, to induce oxidative stress in NP cells. Stimulation with IL-1β contributes to intracellular oxidative stress because it stimulates the production of H_2O_2,[75] $^{\cdot}OH$[76] and $^{\cdot}O_2^-$ [77] radicals by cells. Briefly, IL-1β interacts with its cell surface receptor and activates a cascade of intracellular reactions that activates several signal transduction pathways such as NF-κB and MAPK.[78, 79] As a result, the expression of several enzymes that are associated with the generation of ROS is upregulated.[80] The NADPH oxidases (NOX), a membrane enzyme that produces superoxide, has been found to mediate the generation of ROS by several cell types stimulated with IL-1β.[81] In a study carried out by Rousset *et al.*,[82] NOX4 was identified as the main NOX isoform in human chondrocytes. Expression of

NOX4 and the consequent generation of ROS was upregulated after stimulating the cells with IL-1β.

3.3.4. Expression of Proteolytic Enzymes (MMP-3 and ADAMTS-5)

The expression of MMP-3 and ADAMTS-5 of NP cells in basal conditions or cells stimulated with IL-1β in the absence or presence of 400 μg/mL of catalase-loaded (CAT) or catalase-loaded and tannic acid-functionalized (TA+CAT) capsules was evaluated via qRT-PCR. The results displayed in Figure 5c were normalised with respect to NP cells under basal conditions and to the house-keeping gene (18S). Stimulation of NP cells with 10 ng/mL of IL-1β clearly upregulated the mRNA expression of both proteolytic enzymes. In this case, a 48.8±11.5-fold and a 9.1±0.7-fold increase for MMP-3 and ADAMTS-5 respectively, was observed in those cells stimulated with IL-1β with respect to NP cells under basal conditions. The treatment with catalase-loaded capsules (CAT) significantly downregulated the expression of both enzymes and, accordingly, a 27.5±6.8-fold and a 4.1±0.5-fold increase for MMP-3 and ADAMTS-5 was observed with respect to NP cells under basal conditions. Treatment with catalase-loaded and tannic acid-functionalised (TA+CAT) capsules proved more effective in downregulating the expression of both enzymes. In this situation, a 21.4±1.4-fold and a 3.5±1.9-fold increase was observed with respect to NP cells under basal conditions.

MMPs and ADAMTSs are the major proteolytic enzymes in the IVD and, in the non-degenerated disc, contribute to normal tissue repair and remodelling.[83] However, in the degenerated disc, the expression of these proteolytic enzymes is upregulated over the natural inhibitors such as tissue inhibitor of metalloproteinases (TIMP), which causes a dysregulation of the homeostasis mechanism and results in disc degeneration.[84] MMP-3

proteolyses several components of the extracellular matrix of the disc such as proteoglycans, gelatins and collagens, whereas ADAMTS-5 has shown aggrecanolytic properties. It has been reported that stimulation of NP and AF cells with IL-1β highly upregulates the expression of MMP-3 and ADAMTS-5 due to activation of the NF-κB and MAPK signalling pathways.[66, 67] On the other hand, it has been demonstrated that excessive ROS promotes a catabolic phenotype in NP and AF cells.[74, 85] For example, the expression of MMP-3 was significantly upregulated in AF cells that were stimulated with 100 μM H_2O_2.[85] Interestingly, treatment with an antioxidant (N-acetyl cysteine) down-regulated the expression of MMP-3 with respect to untreated cells. Similar results were reported in another study, where the up-regulation of MMP-3 was reported in NP cells that were stimulated with 100 μM H_2O_2.[74] Again, the treatment with an antioxidant compound (ferulic acid) efficiently attenuated the expression of MMP-3. In summary, oxidative stress and inflammation causes an imbalance in the matrix homeostasis with an increased expression of proteolytic enzymes and a decrease in the levels of matrix components (including aggrecan, collagen)[86] that results in disc degeneration. Therefore, treatments that target the excess ROS may represent a promising strategy to prevent disc degeneration.

4. Conclusions

In the present work, we fabricated polymer capsules loaded with catalase and functionalized with an external layer of TA via the LbL approach. Catalase remained active inside the polymer capsules and was able to scavenge H_2O_2 from solution, while the external layer of TA showed intrinsic antioxidant properties, being able to scavenge both H_2O_2 and $^{\cdot}OH$. The fabricated polymer capsules were applied in an IL-1β induced NP inflammation model to evaluate their potential to prevent oxidative stress. Polymer

capsules were uptaken by NP cells and their presence did not negatively affect the metabolic activity nor the viability of the cells. The levels of intracellular ROS in IL-1β stimulated cells were reduced by the presence of the polymer capsules, which demonstrated their potential to prevent oxidative stress. Additionally, the expression of two major proteolytic enzymes (MMP-3 and ADAMTS-5) was attenuated in the presence of the polymer capsules.

Acknowledgments

This publication has emanated from research conducted with the financial support of Science Foundation Ireland (SFI) and is co-funded under the European Regional Development Programme under Grant Number 13/RC/2073. A.L. and J.R.S. would like to acknowledge the Basque Government (Department of Education, Language Policy and Culture) for a postdoctoral grant and project GIC IT-632-13 respectively. The Spanish Ministry of Industry and Competitiveness for project MAT 2013-45559-P is also acknowledged. S.T., M.L. and C.P. gratefully acknowledge the financial support provided by the University of Basel and the Swiss National Science Foundation (SNSF). A.P. and J.R.S would like to acknowledge the European Cooperation in Science and Technology (COST) Action iPROMEDAI project (TD 1305). We acknowledge the editorial assistance of Mr Keith Feerick and Maciej Doczyk for his support in the preparation of the figures in this manuscript. We wish to thank Diana R. Pereira for her assistance with the experimental design and analysis of flow cytometry results. We also acknowledge Pascal Richard for his technical assistance in EPR.

Conflicts of Interest

There are no conflicts to declare.

References

1. B. C. Dash, S. Mahor, O. Carroll, A. Mathew, W. Wang, K. A. Woodhouse, A. Pandit, Tunable elastin-like polypeptide hollow sphere as a high payload and controlled delivery gene depot. J. Control. Release. 152 (2011) 382-392.
2. B. C. Dash, D. Thomas, M. Monaghan, O. Carroll, X. Chen, K. Woodhouse, T. O'Brien, A. Pandit, Biomaterials. 65 (2015) 126-139.
3. S. Browne, M. G. Monaghan, E. Brauchle, D. C. Berrio, S. Chantepie, D. Papy-Garcia, K. Schenke-Layland, A. Pandit, Modulation of inflammation and angiogenesis and changes in ECM GAG-activity via dual delivery of nucleic acids, Biomaterials. 69 (2015) 133-147.
4. B. Iyisan, J. Kluge, P. Formanek, B. Voit, D. Appelhans, Multifunctional and dual-responsive polymersomes as robust nanocontainers: design, formation by sequential post-conjugations, and pH-controlled drug release, Chem. Mater. 28 (2016) 1513-1525.
5. F. Liu, V. Kozlovskaya, S. Medipelli, B. Xue, F. Ahmad, M. Saeed, D. Cropek, E. Kharlampieva, Temperature-sensitive polymersomes for controlled delivery of anticancer drugs, Chem. Mater. 27 (2015) 7945-7956.
6. W.-C. Liao, Y. S. Sohn, M. Riutin, A. Cecconello, W. J. Parak, R. Nechushtai, I. Willner, The application of stimuli‐responsive VEGF- and ATP-aptamer‐based microcapsules for the controlled release of an anticancer drug, and the selective targeted cytotoxicity toward cancer cells, Adv. Funct. Mater. 26 (2016) 4262-4273.
7. M. Marguet, C. Bonduelle, S. Lecommandoux, Multicompartmentalized polymeric systems: towards biomimetic cellular structure and function, Chem. Soc. Rev. 42 (2013) 512-529.
8. B. Städler, A. D. Price, A. N. Zelikin, A critical look at multilayered polymer capsules in biomedicine: drug carriers, artificial organelles, and cell mimics, Adv. Funct. Mater. 21 (2011) 14-28.
9. C. G. Palivan, R. Goers, A. Najer, X. Zhang, A. Car, W. Meier, Bioinspired polymer vesicles and membranes for biological and medical applications, Chem. Soc. Rev. 45(2) (2016) 377-411.
10. J. Gaitzsch, X. Huang, B. Voit, Engineering functional polymer capsules toward smart nanoreactors, Chem. Rev. 116 (2016) 1053-1093.
11. A. Larrañaga, M. Lomora, J. R. Sarasua, C. G. Palivan, A. Pandit, Polymer capsules as micro-/nanoreactors for therapeutic applications: current strategies to control membrane permeability, Prog. Mater. Sci. 90 (2017) 325-357.
12. S. F. van Dongen, M. Nallani, J. J. Cornelissen, R. J. Nolte, J. C. van Hest, A three-enzyme cascade reaction through positional assembly of enzymes in a polymersome nanoreactor, Chemistry. 15 (2009) 1107-1114.
13. D. M. Vriezema, P. M. L. Garcia, N. Sancho Oltra, N. S. Hatzakis, S. M. Kuiper, R. J. M. Nolte, A. E. Rowan, J. C. M. van Hest, Positional assembly of enzymes in polymersome nanoreactors for cascade reactions. Angew. Chem. 46 (2007) 7378-7382.
14. C. G. Palivan, O. Fischer-Onaca, M. Delcea, F. Itel, W. Meier, Protein-polymer nanoreactors for medical applications, Chem. Soc. Rev. 41 (2012) 2800-2823.
15. C. Nardin, J. Widmer, M. Winterhalter, W. Meier, Amphiphilic block copolymer nanocontainers as bioreactors, Eur. Phys. J.E. 4 (2001) 403-410.

16. M. Spulber, P. Baumann, J. Liu, C. G. Palivan, Ceria loaded nanoreactors: a nontoxic superantioxidant system with high stability and efficacy, Nanoscale. 7 (2015) 1411-1423.
17. P. Tanner, V. Balasubramanian, C. G. Palivan, Aiding nature's organelles: artificial peroxisomes play their role, Nano. Lett. 13 (2013) 2875-2883.
18. P. Tanner, O. Onaca, V. Balasubramanian, W. Meier, C. G. Palivan, Enzymatic cascade reactions inside polymeric nanocontainers: a means to combat oxidative stress, Chem. Eur. J. 17 (2011) 4552-4560.
19. K. Langowska, C. G. Palivan, W. Meier, Polymer nanoreactors shown to produce and release antibiotics locally, Chem. Commun. 49 (2013) 128-130.
20. M. Lomora, M. Garni, F. Itel, P. Tanner, M. Spulber, C. G. Palivan, Polymersomes with engineered ion selective permeability as stimuli-responsive nanocompartments with preserved architecture, Biomaterials. 53 (2015) 406-414.
21. Y. Zhu, F. Wang, C. Zhang, J. Du, Preparation and mechanism insight of nuclear envelope-like polymer vesicles for facile loading of biomacromolecules and enhanced biocatalytic activity, ACS. Nano. 8 (2014) 6644-6654.
22. D. Grafe, J. Gaitzsch, D. Appelhans, B. Voit, Cross-linked polymersomes as nanoreactors for controlled and stabilized single and cascade enzymatic reactions, Nanoscale. 6 (2014) 10752-10761.
23. C. Gao, X. Liu, J. Shen, H. Mohwald, Spontaneous deposition of horseradish peroxidase into polyelectrolyte multilayer capsules to improve its activity and stability, Chem. Commun. 17 (2002) 1928-1929.
24. N. G. Balabushevich, O. P. Tiourina, D. V. Volodkin, N. I. Larionova, G. B. Sukhorukov, Loading the multilayer dextran sulfate/protamine microsized capsules with peroxidase, Biomacromolecules. 4 (2003) 1191-1197.
25. O. P. Tiourina, A. A. Antipov, G. B. Sukhorukov, N. I. Larionova, Y. Lvov, H. Möhwald, Entrapment of α-chymotrypsin into hollow polyelectrolyte microcapsules, Macromol. Biosci. 1 (2001) 209-214.
26. D. Valdeperez, P. Del Pino, L. Sanchez, W. J. Parak, B. Pelaz, Highly active antibody-modified magnetic polyelectrolyte capsules, J. Colloid. Interface. Sci. 474 (2016) 1-8.
27. S. Carregal-Romero, P. Guardia, X. Yu, R. Hartmann, T. Pellegrino, W. J. Parak, Magnetically triggered release of molecular cargo from iron oxide nanoparticle loaded microcapsules, Nanoscale. 7 (2015) 570-576.
28. S. Donatan, A. Yashchenok, N. Khan, B. Parakhonskiy, M. Cocquyt, B.-E. Pinchasik, D. Khalenkow, H. Möhwald, M. Konrad, A. Skirtach, Loading capacity versus enzyme activity in anisotropic and spherical calcium carbonate microparticles, ACS. Appl. Mater. Interfaces. 8 (2016) 14284-14292.
29. C. Hou, Y. Wang, H. Zhu, L. Zhou, Formulation of robust organic–inorganic hybrid magnetic microcapsules through hard-template mediated method for efficient enzyme immobilization, J. Mater. Chem. B. 3 (2015) 2883-2891.
30. J. Shi, C. Yang, S. Zhang, X. Wang, Z. Jiang, W. Zhang, X. Song, Q. Ai, C. Tian, Polydopamine microcapsules with different wall structures prepared by a template-mediated method for enzyme immobilization. ACS. Appl. Mater. Interfaces. 5 (2013) 9991-9997.
31. J. Shi, W. Zhang, S. Zhang, X. Wang, Z. Jiang, Synthesis of organic-inorganic hybrid microcapsules through in situ generation of an inorganic layer on an adhesive layer with mineralization-inducing capability, J. Mater. Chem. B. 3 (2015) 465-474.

32. C. S. Karamitros, A. M. Yashchenok, H. Möhwald, A. G. Skirtach, M. Konrad, Preserving catalytic activity and enhancing biochemical stability of the therapeutic enzyme asparaginase by biocompatible multilayered polyelectrolyte microcapsules, Biomacromolecules. 14 (2013) 4398-4406.
33. M. Valko, D. Leibfritz, J. Moncol, M. T. Cronin, M. Mazur, J. Telser, Free radicals and antioxidants in normal physiological functions and human disease, Int. J. Biochem. Cell. Biol. 39 (2007) 44-84.
34. C. Tapeinos, A. Pandit, Physical, chemical, and biological structures based on ros-sensitive moieties that are able to respond to oxidative microenvironment, Adv. Mater. 28 (2016) 5553-5585.
35. S. G. Rhee, Redox signaling: hydrogen peroxide as intracellular messenger, Exp. Mol. Med. 31(2) (1999) 53-59.
36. M. Valko, C. J. Rhodes, J. Moncol, M. Izakovic, M. Mazur, Free radicals, metals and antioxidants in oxidative stress-induced cancer, Chem.Biol. Interact. 160 (2006) 1-40.
37. S. Reuter, S. C. Gupta, M. M. Chaturvedi, B. B. Aggarwal, Oxidative stress, inflammation, and cancer: how are they linked? Free. Radical. Biol. Med. 49(11) (2010) 1603-1616.
38. M. T. Lin, M. F. Beal, Mitochondrial dysfunction and oxidative stress in neurodegenerative diseases, Nature, 443(7113) (2006) 787-795.
39. K. M. Poole, C. E. Nelson, R. V. Joshi, J. R. Martin, M. K. Gupta, S. C. Haws, T. E. Kavanaugh, M. C. Skala, C. L. Duvall, ROS-responsive microspheres for on demand antioxidant therapy in a model of diabetic peripheral arterial disease, Biomaterials, 41 (2015) 166-175.
40. A. Dimozi, E. Mavrogonatou, A. Sklirou, D. Kletsas, Oxidative stress inhibits the proliferation, induces premature senescence and promotes a catabolic phenotype in human nucleus pulposus intervertebral disc cells, Eur. Cells. Mater. 30 (2015) 89-103.
41. J. W. Chen, B. B. Ni, B. Li, Y. H. Yang, S. D. Jiang, L. S. Jiang, The responses of autophagy and apoptosis to oxidative stress in nucleus pulposus cells: implications for disc degeneration, Cell. Physiol. Biochem. 34 (2014) 1175-1189.
42. L. A. Nasto, A. R. Robinson, K. Ngo, C. L. Clauson, Q. Dong, C. St Croix, G. Sowa, E. Pola, P. D. Robbins, J. Kang, L. J. Niedernhofer, P. Wipf, N. V. Vo, Mitochondrial-derived reactive oxygen species (ROS) play a causal role in aging-related intervertebral disc degeneration, J. Orthop. Res. 31 (2013) 1150-1157.
43. L. Poveda, M. Hottiger, N. Boos, K. Wuertz, Peroxynitrite induces gene expression in intervertebral disc cells, Spine. 34 (2009) 1127-1133.
44. K. Takahashi, Y. Aoki, S. Ohtori, Resolving discogenic pain, Eur. Spine. J. 17(S4) (2008) 428-431.
45. B. Peng, J. Hao, S. Hou, W. Wu, D. Jiang, X. Fu, Y. Yang, Possible pathogenesis of painful intervertebral disc degeneration, Spine. 31(5) (2006) 560-566.
46. I. L. M. Isa, A. Srivastava, D. Tiernan, P. Owens, P. Rooney, P. Dockery, A. Pandit, Hyaluronic acid based hydrogels attenuate inflammatory receptors and neurotrophins in interleukin-1β induced inflammation model of nucleus pulposus cells, Biomacromolecules. 16(6) (2015) 1714-1725.

47. M. M. Bradford, A rapid and sensitive method for the quantitation of microgram quantities of protein utilizing the principle of protein-dye binding, Anal. Biochem. 72 (1976) 248-254.
48. A. Srivastava, I. L. Isa, P. Rooney, A. Pandit, Bioengineered three-dimensional diseased intervertebral disc model revealed inflammatory crosstalk, Biomaterials. 123 (2017) 127-141.
49. D. V. Volodkin, N. I. Larionova, G. B. Sukhorukov, Protein encapsulation via porous CaCO3 microparticles templating, Biomacromolecules. 5(5) (2004) 1962-1972.
50. A. I. Petrov, D. V. Volodkin, G. B. Sukhorukov, Protein-calcium carbonate coprecipitation: a tool for protein encapsulation, Biotechnol. Prog. 21(3) (2005) 918-925.
51. M.-L. De Temmerman, J. Demeester, F. De Vos, S. C. De Smedt, Encapsulation performance of layer-by-layer microcapsules for proteins, Biomacromolecules. 12(4) (2011) 1283-1289.
52. T. Shutava, M. Prouty, D. Kommireddy, Y. Lvov, pH responsive decomposable layer-by-layer nanofilms and capsules on the basis of tannic acid, Macromolecules. 38(7) (2005) 2850-2858.
53. J.M. Matés, Effects of antioxidant enzymes in the molecular control of reactive oxygen species toxicology, Toxicology. 153(1-3) (2000) 83-104.
54. S. Shu, C. Sun, X. Zhang, Z. Wu, Z. Wang, C. Li, Hollow and degradable polyelectrolyte nanocapsules for protein drug delivery, Acta. Biomater. 6 (2010) 210-217.
55. S. Yan, J. Zhu, Z. Wang, J. Yin, Y. Zheng, X. Chen, Layer-by-layer assembly of poly(L-glutamic acid)/chitosan microcapsules for high loading and sustained release of 5-fluorouracil, Eur. J. Pharm. Biopharm. 78(3) (2011) 336-345.
56. C. de Gracia Lux, S. Joshi-Barr, T. Nguyen, E. Mahmoud, E. Schopf, N. Fomina, A. Almutairi, Biocompatible polymeric nanoparticles degrade and release cargo in response to biologically relevant levels of hydrogen peroxide, J. Am. Chem. Soc. 134(38) (2012) 15758-15764.
57. İ. Gülçin, Z. Huyut, M. Elmastaş, H. Y. Aboul-Enein, Radical scavenging and antioxidant activity of tannic acid, Arabian. J. Chem. 3(1) (2010) 43-53.
58. N. P. Morales, S. Sirijaroonwong, P. Yamanont, C. Phisalaphong, Electron paramagnetic resonance study of the free radical scavenging capacity of curcumin and its demethoxy and hydrogenated derivative, Biol. Pharm. Bull. 38(10) (2015) 1478-1483.
59. G. K. B. Lopes, H. M. Schulman, M. Hermes-Lima, Polyphenol tannic acid inhibits hydroxyl radical formation from Fenton reaction by complexing ferrous ions, Biochim. Biophys. Acta. 1472 (1-2) (1999) 142-152.
60. N. Loganayaki, P. Siddhuraju, S. Manian, Antioxidant activity and free radical scavenging capacity of phenolic extracts from Helicteres isora L. and Ceiba pentandra L, J. Food Sci. Technol. 50(4) (2013) 687-695.
61. T.G. Shutava, M.D. Prouty, V.E. Agabekov, Y.M. Lvov, Antioxidant properties of layer-by-layer films on the basis of tannic acid, Chem. Lett. 35(10) (2006) 1144-1145.
62. M. V. Lomova, G. B. Sukhorukov, M. N. Antipina, Antioxidant coating of micronsize droplets for prevention of lipid peroxidation in oil-in-water emulsion, ACS Appl. Mater. Interfaces. 2(12) (2010) 3669-3676.
63. D. M. O'Halloran, A. S. Pandit, Tissue-engineering approach to regenerating the intervertebral disc, Tissue Eng. 13(8) (2007) 1927-1954.

64. N. D. Perkins, Integrating cell-signalling pathways with NF-kappaB and IKK function, Nat. Rev. Mol. Cell Biol. 8(1) (2007) 49-62.
65. T. D. Gilmore, Introduction to NF-kappaB: players, pathways, perspectives, Oncogene. 25(51) (2006) 6680-6684.
66. Q. Liu, L. Jin, F. H. Shen, G. Balian, X. J. Li, Fullerol nanoparticles suppress inflammatory response and adipogenesis of vertebral bone marrow stromal cells--a potential novel treatment for intervertebral disc degeneration, Spine. J. 13(11) (2013) 1571-1580.
67. W. Yang, X. H. Yu, C. Wang, W. S. He, S. J. Zhang, Y. G. Yan, J. Zhang, Y. X. Xiang, W. J. Wang, Interleukin-1β in intervertebral disk degeneration, Clin. Chim. Acta. 450 (2015) 262-272.
68. R. Hartmann, M. Weidenbach, M. Neubauer, A. Fery, W. J. Parak, Stiffness-dependent in vitro uptake and lysosomal acidification of colloidal particles, Angew. Chem. 54 (2015) 1365-1368.
69. L. L. del Mercato, F. Guerra, G. Lazzari, C. Nobile, C. Bucci, R. Rinaldi, Biocompatible multilayer capsules engineered with a graphene oxide derivative: synthesis, characterization and cellular uptake., Nanoscale. 8 (2016) 7501-7512.
70. H. Li, W. Zhang, W. Tong, C. Gao, Enhanced cellular uptake of bowl-like microcapsules, ACS. Appl. Mater. Interfaces. 8 (2016) 11210-11214.
71. H. Gao, O. A. Goriacheva, N. V. Tarakina, G. B. Sukhorukov, Intracellularly biodegradable polyelectrolyte/silica composite microcapsules as carriers for small molecules, ACS. Appl. Mater. Interfaces. 8 (2016) 9651-9661.
72. A. M. Pavlov, A. V. Sapelkin, X. Huang, M. P'Ng K, A. J. Bushby, G. B. Sukhorukov, A. G. Skirtach, Neuron cells uptake of polymeric microcapsules and subsequent intracellular release, Macromol. Biosci. 11 (2011) 848-854.
73. L. Yang, Z. Rong, M. Zeng, Y. Cao, X. Gong, L. Lin, Y. Chen, W. Cao, L. Zhu, W. Dong, Pyrroloquinoline quinone protects nucleus pulposus cells from hydrogen peroxide-induced apoptosis by inhibiting the mitochondria-mediated pathway, Eur. Spine J. 24 (2015) 1702-1710.
74. Y.-H. Cheng, S.-H. Yang, K.-C. Yang, M.-P. Chen, F.-H. Lin, The effects of ferulic acid on nucleus pulposus cells under hydrogen peroxide-induced oxidative stress, Process Biochem. 46(8) (2011) 1670-1677.
75. A. F. Mendes, M. M. Caramona, A. P. Carvalho, M. C. Lopes, Differential roles of hydrogen peroxide and superoxide in mediating IL-1-induced NF-kappa B activation and iNOS expression in bovine articular chondrocytes, J. Cell. Biochem. 88 (2003) 783-793.
76. M. L. Tiku, Y. P. Yan, K. Y. Chen, Hydroxyl radical formation in chondrocytes and cartilage as detected by electron paramagnetic resonance spectroscopy using spin trapping reagents, Free. Radical. Res. 29 (1998) 177-187.
77. T. Tawara, M. Shingu, M. Nobunaga, T. Naono, Effects of recombinant human IL-1 beta on production of prostaglandin E2, leukotriene B4, NAG, and superoxide by human synovial cells and chondrocytes, Inflammation. 15 (1991) 145-157.
78. F. Berenbaum, Signaling transduction: target in osteoarthritis, Curr. Opin. Rheumatol. 16 (2004) 616-622.
79. R. K. Studer, L. G. Gilbertson, H. Georgescu, G. Sowa, N. Vo, J. D. Kang, p38 MAPK inhibition modulates rabbit nucleus pulposus cell response to IL-1, J. Orthop. Res. 26 (2008) 991-998.
80. M. J. Morgan, Z. G. Liu, Crosstalk of reactive oxygen species and NF-κB signaling, Cell Res. 21 (2011) 103-115.

81. R. Brigelius-Flohe, A. Banning, M. Kny, G. F. Bol, Redox events in interleukin-1 signaling, Arch. Biochem. Biophys. 423 (2004) 66-73.
82. F. Rousset, F. Hazane-Puch, C. Pinosa, M. V. Nguyen, L. Grange, A. Soldini, B. Rubens-Duval, C. Dupuy, F. Morel, B. Lardy, IL-1beta mediates MMP secretion and IL-1beta neosynthesis via upregulation of p22(phox) and NOX4 activity in human articular chondrocytes, Osteoarthritis and cartilage. 23 (2015) 1972-1980.
83. N. V. Vo, R. A. Hartman, T. Yurube, L. J. Jacobs, G. A. Sowa, J. D. Kang, Expression and regulation of metalloproteinases and their inhibitors in intervertebral disc aging and degeneration, Spine J. 13 (2013) 331-341.
84. C. L. Le Maitre, A. Pockert, D. J. Buttle, A. J. Freemont, J. A. Hoyland, Matrix synthesis and degradation in human intervertebral disc degeneration, Biochem. Soc. Trans. 35 (2007) 652-655.
85. S. Suzuki, N. Fujita, N. Hosogane, K. Watanabe, K. Ishii, Y. Toyama, K. Takubo, K. Horiuchi, T. Miyamoto, M. Nakamura, M. Matsumoto, Excessive reactive oxygen species are therapeutic targets for intervertebral disc degeneration, Arthritis Res. Ther. 17 (2015) 316.
86. D. Yang, D. Wang, A. Shimer, F. H. Shen, X. Li, X. Yang, Glutathione protects human nucleus pulposus cells from cell apoptosis and inhibition of matrix synthesis, Connect. Tissue Res. 55 (2014) 132-139.

Figure Captions

Figure 1: Schematic representation of the experimental work plan. (List of abbreviations: SEM: scanning electron microscopy/TEM: transmission electron microscopy/DLS: dynamic light scattering/ FTIR: Fourier transform infrared spectroscopy/EDX: energy-dispersive X-ray spectroscopy/EPR: electron paramagnetic resonance).

Figure 2: Morphological characterization via SEM (a-c) and TEM (d) of catalase-loaded $CaCO_3$ template (a, b) and polymer capsules (c, d). ζ-potential of catalase-loaded $CaCO_3$ template and particles after each polyelectrolyte deposition step (e). FTIR spectra of polymer capsules before and after EDTA treatment (f); Figure g and h (at higher magnification) represent fluorescent micrographs of FITC-labeled catalase-loaded polymer capsules.

Figure 3: Stopped-flow absorbance measurements with a final H_2O_2 concentration of 10 mM (a). Fluorimetric measurements to determine the H_2O_2 scavenging capacity of the developed capsules (400 µg/mL) at biologically relevant H_2O_2 concentrations (10 µM and 50 µM) (b). Asterisks (*) indicate significant differences ($p<0.05$). EPR spectra of DMPO/˙OH (final H_2O_2 concentration 1 mM) adduct in the presence of several concentrations of polymer capsules (c); the relative concentration of the OH radical (d).

Figure 4: Metabolic activity of NP cells in the presence of polymer capsules (a). Viability of non-stimulated NP cells (b) Viability of NP cells stimulated with IL-1β (c) Viability of NP cells stimulated with IL-1β in the presence of catalase-loaded capsules (d) Viability of NP cells stimulated with IL-1β in the presence of catalase-loaded and

tannic acid-functionalized capsules (e). Fluorescent micrographs of NP cells in the presence of FITC-labelled polymer capsules (f and g) (Nuclei-Hoechst: Blue/Actin filaments-Rhodamine Phalloidin: Red/Polymer capsules-FITC: Green). White arrows highlight the colocalization of FITC-labelled capsules with actin filaments. Representative dot-plot of NP cells in the absence (h-left) or presence (h-middle) of FITC-labelled capsules and the resulting histogram (h-right) (blue-absence of polymer capsules/green-presence of polymer capsules).

Figure 5: Fluorescent micrographs of NP cells (Nuclei-Hoechst: Blue/Actin filaments-Rhodamine Phalloidin: Red/Oxidative Stress-CellROX®: Green) (a) and corresponding quantification (b). Gene expression of MMP-3 and ADAMTS-5 normalized with respect to NP cells under basal conditions and house-keeping gene (18S). Asterisks (*) indicate significant differences ($p<0.05$) with respect to stimulated (i.e., IL-1β treated) cells.

Figure S1: Calibration curve and calculation of catalase encapsulation efficiency via the Bradford assay.

Figure S2: SEM micrographs and EDX spectra of polymer capsules before and after the removal of the $CaCO_3$ template.

Figure S3: Fluorescent micrographs of FITC-labeled catalase-loaded polymer capsules after 0 and 3 days incubated in PBS at 37 ºC.

Figure S4: Fluorimetric measurements to determine the H_2O_2 scavenging capacity of the developed capsules (100 µg/mL and 400 µg/mL) at biologically relevant H_2O_2 concentrations (10 µM and 50 µM). Asterisks (*) indicate significant differences ($p<0.05$) with respect to the control (i.e., empty capsules).

Figure S5: Relative activity of TA+CAT capsules (400 µg/mL) after being submerged in PBS at 37 ºC with respect to TA+CAT capsules non-submerged (day 0) in PBS.

Figure S6: EPR spectra of DMPO/˙OH (final H_2O_2 concentration 1 mM) adduct in the presence of several concentrations of tannic acid and catalase in solution and the relative concentration of the OH radical.

Figure S7: EPR spectra of DMPO/˙OH (final H_2O_2 concentration 100 µM) adduct in the presence of several concentrations of tannic acid and catalase in solution and the relative concentration of the OH radical.

Figure S8: EPR spectra of DMPO/˙OH (final H_2O_2 concentration 100 µM) adduct in the presence of several concentrations of polymer capsules and the relative concentration of the OH radical.

Figure S9: Western blotting (a) and densitometry analysis (b) of NP cells stimulated with IL-1β in the presence of polymeric capsules with respect to non-stimulated NP cells. Secretion of IL-6 in the supernatant after NP cells were stimulated with IL-1β and treated with CAT and TA+CAT capsules (c); Schematic representation of the inflammation *in vitro* model employed (d). Asterisks (*) indicate significant differences ($p<0.05$) with respect to NP cells, whereas # indicates significant differences ($p<0.05$) with respect to stimulated (i.e., IL-1β treated) cells.

Figure S10: Metabolic activity of NP cells in the presence of TA+CAT polymer capsules (100 or 400 μg/mL).

Table S1: Primers utilized in qRT-PCR analysis

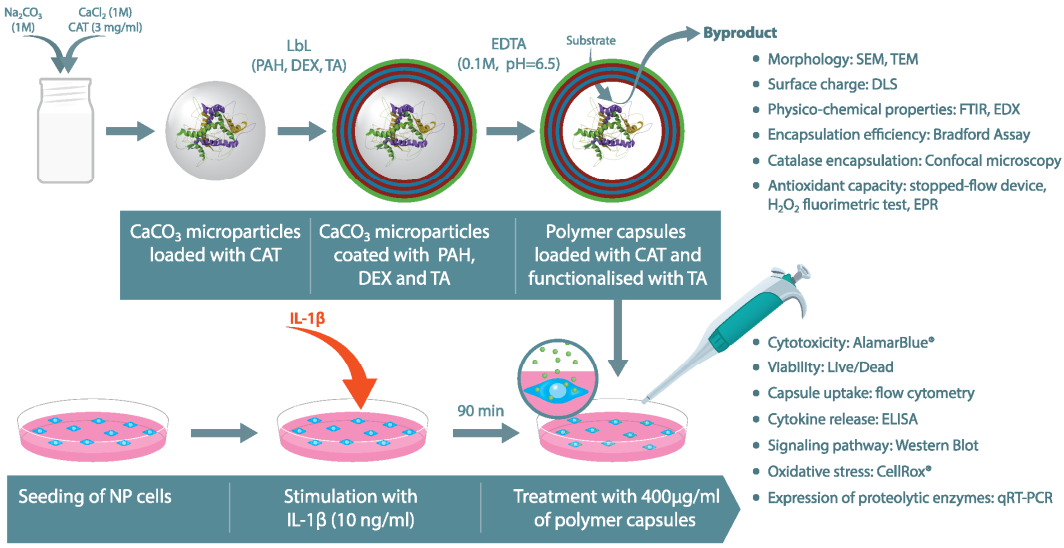
Na_2CO_3 (1M)
$CaCl_2$ (1M) CAT (3 mg/ml)
LbL (PAH, DEX, TA)
EDTA (0.1M, pH=6.5)
Substrate
Byproduct
Morphology: SEM, TEM
Surface charge: DLS
Physico-chemical properties: FTIR, EDX
Encapsulation efficiency: Bradford Assay
Catalase encapsulation: Confocal microscopy
Antioxidant capacity: stopped-flow device, H_2O_2 fluorimetric test, EPR
$CaCO_3$ microparticles loaded with CAT
$CaCO_3$ microparticles coated with PAH, DEX and TA
Polymer capsules loaded with CAT and functionalised with TA
IL-1β
90 min
Cytotoxicity: AlamarBlue®
Viability: Live/Dead
Capsule uptake: flow cytometry
Cytokine release: ELISA
Signaling pathway: Western Blot
Oxidative stress: CellRox®
Expression of proteolytic enzymes: qRT-PCR
Seeding of NP cells
Stimulation with IL-1β (10 ng/ml)
Treatment with 400µg/ml of polymer capsules

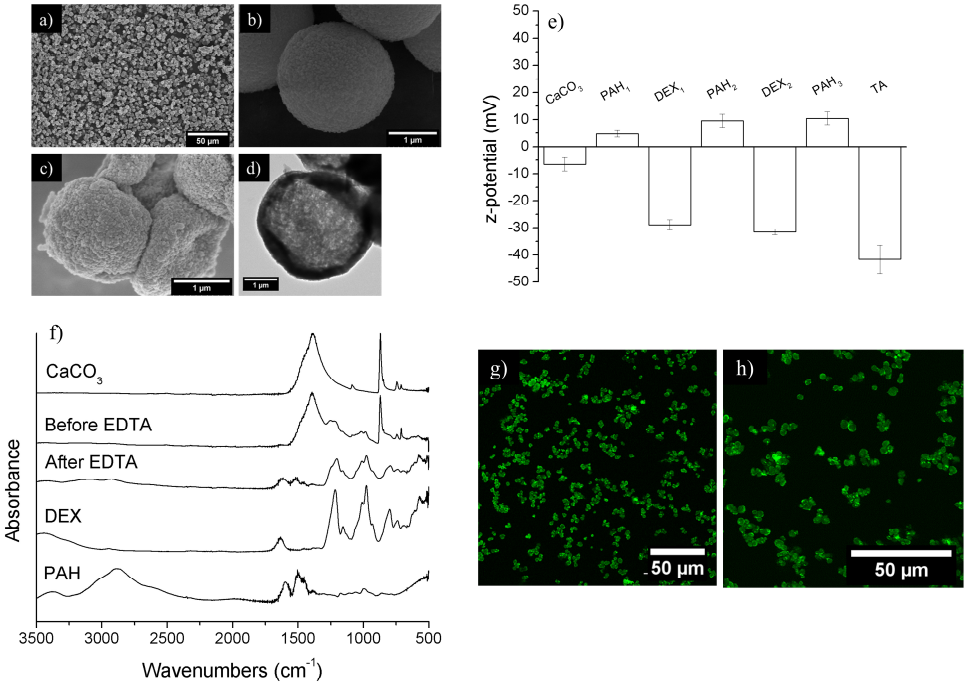
a)
50 µm
b)
1 µm
c)
1 µm
d)
1 µm
e)
z-potential (mV)
50
40
30
20
10
0
-10
-20
-30
-40
-50
CaCO3
PAH1
DEX1
PAH2
DEX2
PAH3
TA
f)
CaCO3
Before EDTA
After EDTA
DEX
PAH
Absorbance
3500
3000
2500
2000
1500
1000
500
Wavenumbers (cm-1)
g)
50 µm
h)
50 µm

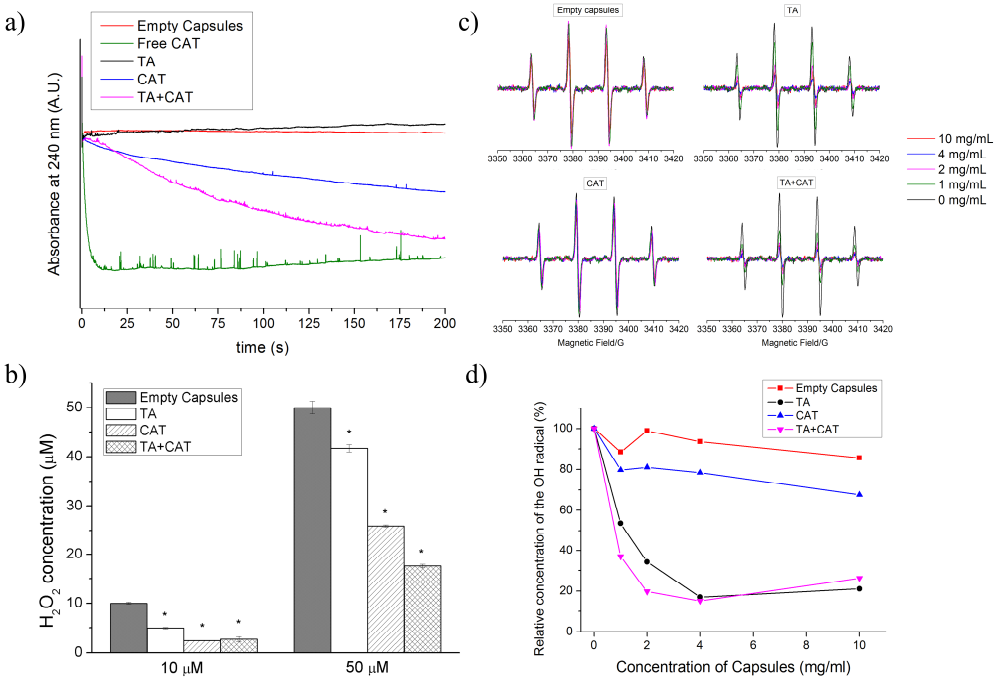
a)
Empty Capsules
Free CAT
TA
CAT
TA+CAT
Absorbance at 240 nm (A.U.)
time (s)
c)
Empty capsules
TA
CAT
TA+CAT
10 mg/mL
4 mg/mL
2 mg/mL
1 mg/mL
0 mg/mL
Magnetic Field/G
b)
Empty Capsules
TA
CAT
TA+CAT
H2O2 concentration (μM)
10 μM
50 μM
d)
Empty Capsules
TA
CAT
TA+CAT
Relative concentration of the OH radical (%)
Concentration of Capsules (mg/ml)

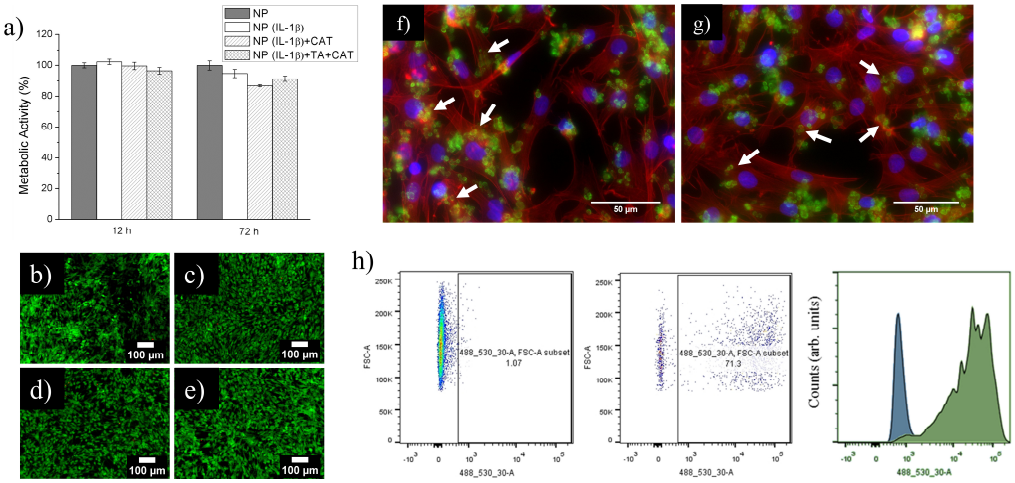
a)
NP
NP (IL-1β)
NP (IL-1β)+CAT
NP (IL-1β)+TA+CAT
Metabolic Activity (%)
120
100
80
60
40
20
0
12 h
72 h
b)
c)
d)
e)
100 μm
f)
g)
50 μm
h)
FSC-A
488_530_30-A, FSC-A subset
1.07
71.3
488_530_30-A
Counts (arb. units)

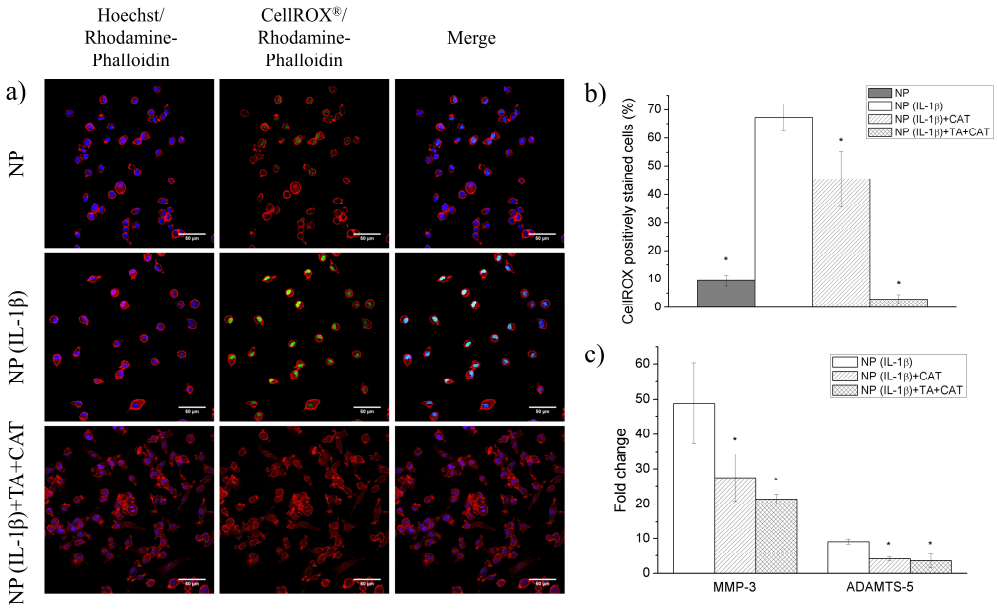
a)
Hoechst/ Rhodamine-Phalloidin
CellROX®/ Rhodamine-Phalloidin
Merge
NP
NP (IL-1β)
NP (IL-1β)+TA+CAT
b)
CellROX positively stained cells (%)
NP
NP (IL-1β)
NP (IL-1β)+CAT
NP (IL-1β)+TA+CAT
c)
Fold change
NP (IL-1β)
NP (IL-1β)+CAT
NP (IL-1β)+TA+CAT
MMP-3
ADAMTS-5

Oxidative stress damages important cell structures leading to cellular apoptosis and senescence, for numerous disease pathologies including cancer, neurodegeneration or osteoarthritis. Thus, the development of biomaterials-based systems to control oxidative stress has gained an increasing interest. Herein, polymer capsules loaded with catalase and functionalized with an external layer of tannic acid are fabricated, which can efficiently scavenge important reactive oxygen species (i.e., hydroxyl radicals and hydrogen peroxide) and modulate extracellular matrix activity in an *in vitro* inflammation model of nucleus pulposus. The present work represents accordingly, an important advance in the development and application of polymer capsules with antioxidant properties for the treatment of oxidative stress, which is applicable for multiple inflammatory disease targets.

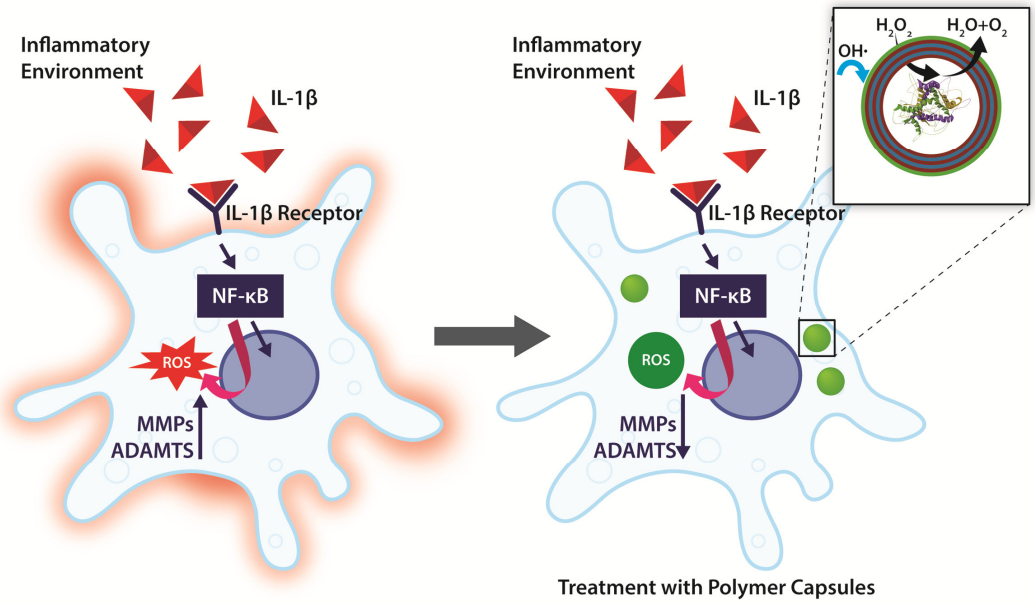
Inflammatory Environment
IL-1β
IL-1β Receptor
NF-κB
ROS
MMPs ADAMTS
Inflammatory Environment
IL-1β
IL-1β Receptor
NF-κB
ROS
MMPs ADAMTS
H_2O_2
H_2O+O_2
OH·
Treatment with Polymer Capsules